Low-energy structure of $^{66}_{27}Co_{39}$ and $^{68}_{27}Co_{41}$ populated through β decay

S. N. Liddick,[1,2] B. Abromeit,[1] A. Ayres,[3] A. Bey,[3] C. R. Bingham,[3] M. Bolla,[1] L. Cartegni,[3] H. L. Crawford,[4] I. G. Darby,[5] R. Grzywacz,[3] S. Ilyushkin,[6] N. Larson,[1,2] M. Madurga,[3] D. Miller,[3] S. Padgett,[3] S. Paulauskas,[3] M. M. Rajabali,[5] K. Rykaczewski,[7] and S. Suchyta[1,2]

[1]*National Superconducting Cyclotron Laboratory (NSCL), Michigan State University, East Lansing, Michigan 48824, USA*
[2]*Department of Chemistry, Michigan State University, East Lansing, Michigan 48824, USA*
[3]*Department of Physics and Astronomy, University of Tennessee, Knoxville, Tennessee 37996, USA*
[4]*Nuclear Science Division, Lawrence Berkeley National Laboratory, Berkeley, California 94720, USA*
[5]*Instituut voor Kern- en Stralingsfysica, Katholieke Universiteit Leuven, B-3001 Leuven, Belgium*
[6]*Department of Physics and Astronomy, Mississippi State University, Mississippi 39762, USA*
[7]*Physics Division, Oak Ridge National Laboratory, Oak Ridge, Tennessee 37831, USA*

(Received 13 December 2011; published 30 January 2012)

The low-energy level structures for the neutron-rich Co isotopes at $N = 39$ and $N = 41$ are constructed following the beta decay of the respective even-even Fe isotopes. Spin and parity assignments of the lowest energy populated state in ^{66}Co and ^{68}Co are consistent with a 1^+ spin and parity assignment and attributed to the coupling of the deformed proton configurations identified in ^{67}Co and deformed neutron configurations inferred from neighboring Fe isotones. Comparisons along the $N = 39$ and $N = 41$ isotonic chains reveal a similarity in the structures of the Co and Mn isotopes.

DOI: 10.1103/PhysRevC.85.014328 PACS number(s): 21.10.−k, 23.40.−s, 23.20.−g, 27.50.+e

I. INTRODUCTION

The nature of neutron-rich nuclei below ^{68}Ni has been an ongoing question since it was first proposed that $N = 40$ was a subshell closure. The claim for an $N = 40$ subshell closure was based on the observation of a low-energy 0^+ excited state [1], a high-energy first-excited 2^+ state, E(2^+_1) [2], and a low B($E2$) value between the first excited state and the ground state in ^{68}Ni [3,4]. Microscopically, an $N = 40$ subshell closure results from a large energy separation between the neutron pf-shell states and the $g_{9/2}$ single-particle state.

Numerous independent lines of investigation have subsequently demonstrated that the $N = 40$ subshell closure collapses below ^{68}Ni and collective behavior rapidly develops as protons are removed from the $f_{7/2}$ single-particle state. Such behavior is not completely unexpected given the rapid development of collectivity in other regions with the addition or subtraction of a few nucleons [5,6]. Within the $N = 40$ region, the influence of the neutron $g_{9/2}$, and to a lesser extent the $d_{5/2}$, single-particle states on the development of collectivity has been explored theoretically [7–10] and compared to a wealth of experimental signatures in the $_{24}$Cr, $_{25}$Mn, $_{26}$Fe, and $_{27}$Co isotopic chains. The systematics of the E(2^+_1) states in both Fe and Cr isotopes do not display a peak at $N = 40$ [11,12] but monotonically decrease in energy starting at $N = 36$ and $N = 32$, respectively. Positive parity isomeric states attributed to the neutron $g_{9/2}$ single-particle orbital are known in^{59}Cr [13] and ^{65,67}Fe [14–16]. Within the odd-odd ^{58,60,62}Mn isotopes, the energy of the negative parity band heads resulting from the coupling of the $\pi f_{7/2}$ and $\nu g_{9/2}$ single-particle states consistently drops as $N = 40$ is approached [17]. In addition, gross nuclear properties, such as beta-decay half-lives [11] and reaction cross sections [12,18], have hinted at a change in nuclear structure as protons are removed from the Ni isotopes.

It has been suggested that the fragility of the $N = 40$ subshell closure is the result of shape coexistence between spherical and prolate-deformed configurations [15,19,20]. For a review of shape coexistence across a broad range of proton and neutron numbers please see the work of Ref. [21] and references therein. A $1/2^-$ shape isomer was identified in $^{67}_{27}Co_{40}$ a few hundred keV above the spherical $7/2^-$ ground state [19]. Similar proton configurations have since been identified in $^{65}_{27}Co_{38}$ [22]. In ^{64m,66m}Mn, the low-energy level structures were interpreted based on the excited spherical isomeric states decaying to deformed nuclear ground states [20].

The present study reports on the investigation of the low-energy level structure of ^{66}Co and ^{68}Co populated through the beta decay of the respective ^{66}Fe and ^{68}Fe isotopes. Section II provides the experimental details of the present study. The experimental results and the inferred level schemes for ^{66,68}Co are presented in Sec. III. Section IV provides a discussion of the low-energy level structures in the $N = 39$ and $N = 41$ Co isotopes and the isotonic trends with neighboring Ni, Fe, and Mn nuclei. Finally, conclusions are presented in Sec. V.

II. EXPERIMENTAL DESCRIPTION

Radioactive ions from Sc to Ni were produced using the Coupled Cyclotron Facility at the National Superconducting Cyclotron Laboratory by impinging a 130 MeV/A ^{86}Kr primary beam onto a ^{9}Be target located at the object position of the A1900 fragment separator [23]. The fragmentation products were separated using the A1900 and a thin kapton wedge placed at the intermediate dispersive image of the separator. The full 5% momentum acceptance of the A1900 was used for the present study. The radioactive ions were identified event-by-event through measurements of energy loss and time-of-flight. Time-of-flight was measured between

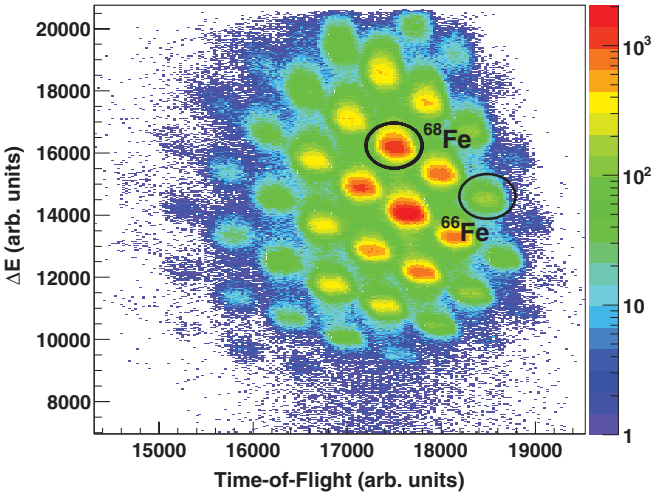

FIG. 1. (Color online) Particle identification plot for the nuclei delivered to the experimental end station characterized on an event-by-event basis using time-of-flight and ΔE techniques. The two beta-decaying Fe isotopes of interest are indicated.

a plastic scintillator at the intermediate dispersive image of the A1900 and a silicon PIN detector placed upstream of the implantation detector. The Si PIN detector also served to measure the energy loss of the incoming ions. The particle identification plot of the nuclei produced during the experiment is shown in Fig. 1. The cocktail beam was delivered to the Beta Counting System (BCS) [24]. The central feature of the BCS is a double-sided silicon strip detector (DSSD). The DSSD, a 1-mm thick, 4 cm × 4 cm wide detector, segmented into 40 1-mm strips on the front and 40 1-mm orthogonal strips on the back, was used to stop the incoming ion beam. The heavy ions were deposited throughout the thickness of the DSSD. Specially designed dual-range preamplifiers were used with the DSSD to detect both the high-energy deposition from the ion-implantation process and the low-energy beta-decay electron. Beta decays were correlated with previously implanted ions based on position and temporal information. Isomeric and beta-delayed gamma rays were monitored with 16 detectors of SeGA [25] arranged in two concentric rings of eight detectors each. The total efficiency of the Ge array was measured to be 8.7% at 662 keV. All detector channels were read out using the the NSCL Digital Data Acquisition System (DDAS) [26]. All channels were individually triggered and time-stamped with a resolution of 10 nanoseconds. Data from the DSSD were written to disk only in the presence of an external validation signal. The validation signal was derived from the coincidence of two distinct OR signals; one OR was generated from all 40 strips on the front of the detector and a second OR was generated from all 40 strips on the back of the detector. The validation signal selected only those events in the DSSD that could be localized to a specific pixel defined by the overlap between a front strip and a back strip. All other detectors were not hardware gated during the experiment. Channels that triggered within a 10-microsecond time window, based on their recorded timestamps, were grouped into an event in software for analysis.

III. RESULTS

A. ^{66}Co

Low-energy states in ^{66}Co were populated following the beta decay of ^{66}Fe. The beta-delayed gamma-ray spectrum observed within 1 second following the implantation of an ^{66}Fe ion is shown in Fig. 2(a). Five gamma rays were identified following the beta decay of ^{66}Fe and are labeled with their energies in Fig. 2(a); their corresponding absolute intensities are presented in Table I. The decay curve, constructed by histogramming the measured time difference between the implantation of a ^{66}Fe ion and the the detection of the subsequent beta-decay electron, is shown in Fig. 2(b). The beta-decay curve was fit with contributions from the decay of ^{66}Fe, ^{66}Co, and a constant background and shows the characteristic behavior expected when the daughter nucleus has a half-life that is shorter than the parent. The half-life of the daughter, ^{66}Co, was fixed in the fit at a value of 180 ms [9,27,28]. The resulting half-life extracted for ^{66}Fe

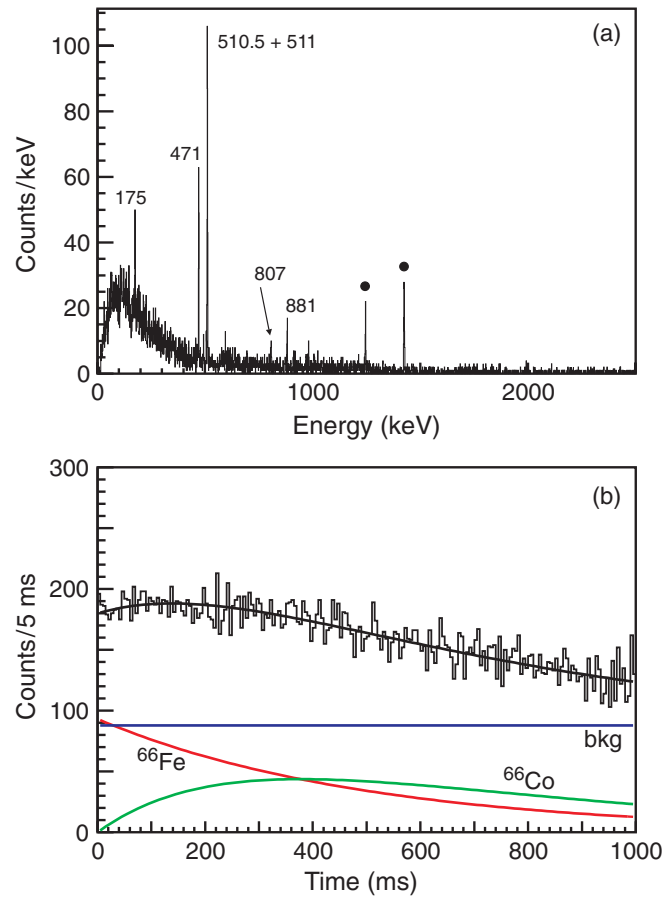

FIG. 2. (Color online) (a) The beta-delayed gamma-ray energy spectrum detected within 1 second following a ^{66}Fe implanted ion. Gamma rays attributed to the decay of ^{66}Fe are labeled with their respective energies. All other gamma rays are assigned to known daughter transitions and are marked by closed circles. (b) The beta-decay curve for ^{66}Co from 0 to 1 second. The overall fit (black) was composed of contributions from the beta decay of ^{66}Fe (red), ^{66}Co (green), and a constant background (blue). See text for details.

TABLE I. Energies and absolute intensities for the gamma-ray transitions identified following the beta decay of ^{66}Fe.

E (keV)	Absolute intensity (%)	E (keV)	Absolute intensity (%)
175.1(3)	6(2)	806.8(4)	5(2)
470.7(3)	15(3)	881.5(3)	8(3)
510.5(5)	14(2)[a]		

[a]Intensity of the 510.5-keV transition extracted from coincidence data. Intensity of the 510.5-keV and 511-keV transitions combined is 34(4)%. See text for details.

was 351 (6) ms consistent with previously obtained literature values [9,29,30].

Coincidences were observed between the 175-keV and 807-keV transitions and the 471-keV and 510.5-keV transitions. The 510.5-keV transition was only identified in the coincidence spectra shown in Fig. 3. Since the 510.5-keV gamma ray could not be resolved from the 511-keV background transition a precise absolute intensity for the transition could not be extracted directly from the beta-gamma spectrum presented in Fig. 2(a). Instead, the absolute intensity was inferred from coincidence spectra. Based on the present data, the order of the 510-keV and 471-keV transitions could not be conclusively determined. Assuming the 471-keV and 510.5-keV transitions are in cascade as depicted in Fig. 4, the

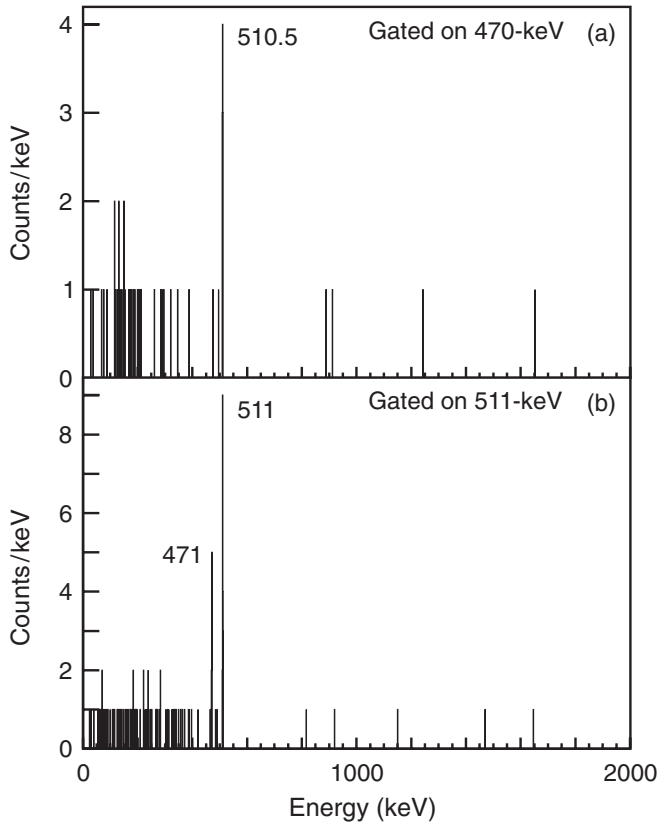

FIG. 3. (a) β-delayed gamma–ray energy spectrum in coincidence with the 471-keV gamma-ray transition. (b) β-delayed gamma–ray energy spectrum in coincidence with the 511-keV gamma-ray transition.

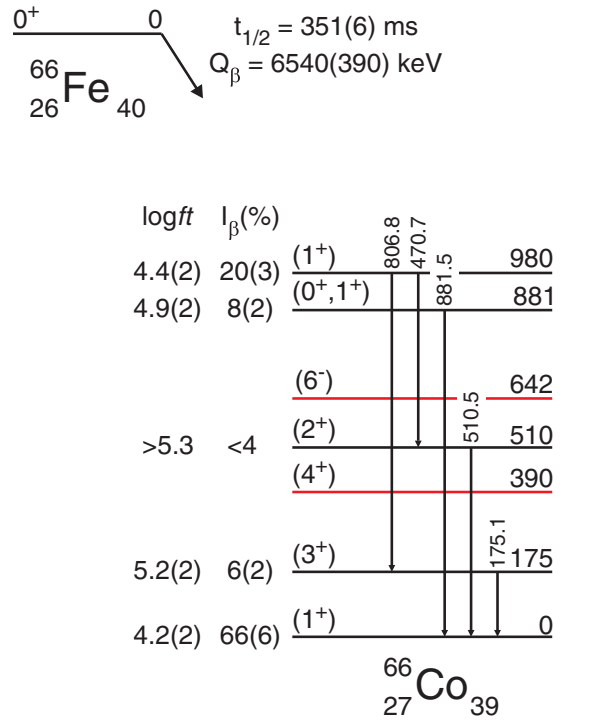

FIG. 4. (Color online) Low-energy level structure of ^{66}Co inferred following the beta decay of ^{66}Fe. Tentative spin and parity assignments, beta-decay branching ratios, and log ft values are given on the left-hand side of each state. States populated through the decay of the 6^- isomer in ^{66}Co which were not observed following beta decay are shown as red lines. The beta-decay Q value of the decay was taken from Ref. [34].

total number of counts expected for a 471-510.5 coincidence was 13(2) based on the observed intensity of the 471-keV transition and the efficiency of SeGA at 510.5 keV. The number of experimentally observed coincidences in Fig. 3(a) is 13(4), placing a lower limit on the absolute intensity of the 510.5-keV transition of 12%, to be consistent with the intensity of the 471-keV at the 1σ level.

The upper absolute intensity limit for the 510.5-keV transition was derived from the gamma-ray spectrum observed in coincidence with the 511-keV transition. The 511-keV coincident gamma-ray spectrum presented in Fig. 3(b) shows two peaks at 471-keV and 511-keV, which can be attributed to the 471-510.5 gamma-ray cascade in ^{66}Co, and the detection of 511-511 coincidence annihilation radiation. The relative ratio of the 471-510.5 coincidences to the sum of the 471-510.5 and 511-511 coincidences is 33(12)%. Again, at the 1σ level, at most, 45% of the total intensity detected in the combined 510.5-keV and 511-keV peak in Fig. 2(a) can be attributed to the 510.5-keV transition. Using the absolute intensity of the combined 511-keV peak given in the footnote of Table I, the upper limit for the absolute intensity of the 510.5-keV transitions is 16%. Based on the lower and upper limits, an absolute intensity of 14(2)% is taken for the 510.5-keV transition.

Combining the absolute gamma-ray intensities and the number of beta decays detected, the beta-decay branching ratios to the observed levels were calculated and are presented

in Fig. 4 along with apparent log ft values. The large apparent direct ground-state-to-ground-state beta-decay branch from ^{66}Fe is inconsistent with the previous 3^+ spin and parity assignment for ^{66}Co [27]. Therefore, the ground state of ^{66}Co is tentatively assigned a spin and parity of 1^+, which was not excluded by the prior study [27] and agrees with recent work presented in Ref. [31]. The reassigned ground-state spin and parity is still consistent with the beta decay of ^{66}Co into ^{66}Ni. Two transitions at 1426 keV and 1246 keV, previously assigned to the decay of ^{66}Co [27] into states of ^{66}Ni, were observed and are shown in Fig. 2(a). The 1426-keV transition is the $2^+ \rightarrow 0^+$ transition in ^{66}Ni. The spin and parity of the 2672-keV state in ^{66}Ni which is depopulated by the 1246-keV transition likely has a spin and parity of 0^+ based on the (t,p) measurements of Ref. [32].

The first excited state of ^{66}Co can be tentatively assigned as a 3^+ state based on the known E2 multipolarity of the isomeric 175-keV transition based on its lifetime of 0.83(1) μs [16,33]. The large beta-decay feeding to the two excited states at 980 keV and 881 keV suggests either a 1^+ or 0^+ spin and parity assignment. A tentative 1^+ assignment for the 980-keV state is preferred and is further discussed in Sec. IV. The state at 510-keV is not directly fed in the beta decay of ^{66}Fe. The state is populated through a transition from the state at 980 keV and then, in turn, decays to the 1^+ ground state suggesting a tentative 2^+ spin and parity assignment. The other two states in ^{66}Co, which were not populated by the beta decay of ^{68}Fe at energies of 390 keV and 642 keV [16], are reassigned as 4^+ and 6^- based on the new ground state spin and parity assignment of ^{66}Co and the expected multipolarities [16].

B. ^{68}Co

Low-energy states in ^{68}Co were populated following the beta decay of ^{68}Fe. The beta-delayed gamma-ray spectrum observed within 1 second following the implantation of a ^{68}Fe ion is shown in Fig. 5(a). All gamma-ray transitions attributed to the decay of ^{68}Fe are listed in Table II with energies and absolute gamma-ray intensities.

There are two beta-decaying states in ^{68}Co that have been identified by their respective beta decays into ^{68}Ni [27]: a 7^- spin and parity ground state and a 3^+ spin and parity isomeric state. Using the selectivity of beta decay, it was possible to exclusively study the states associated with the low-spin isomer. There is no evidence in Fig. 5(a) for the gamma-ray transitions associated with the beta decay of the 7^- ^{68}Co ground state. An upper limit of 2% can be set for the population of the ^{68}Co ground state based on the gamma-ray spectrum shown in Fig. 5 and the known gamma rays in ^{68}Ni [27]. The transitions uniquely attributed to the beta decay of the low-spin Co isomer were observed. The decay curve for ^{68}Fe was extracted and is presented in Fig. 5(b). The decay curve was fit with contributions from the decay of ^{68}Fe, ^{68}Co, and a constant background. The half-life of the daughter ^{68}Co, low-spin, beta-decaying isomeric state was held fixed in the fit at a value of 1.6 seconds [27]. The extracted half-life for ^{68}Fe was 189(6) ms, consistent with previous measurements [8,9,35]. The observed gamma-gamma coincidences are listed

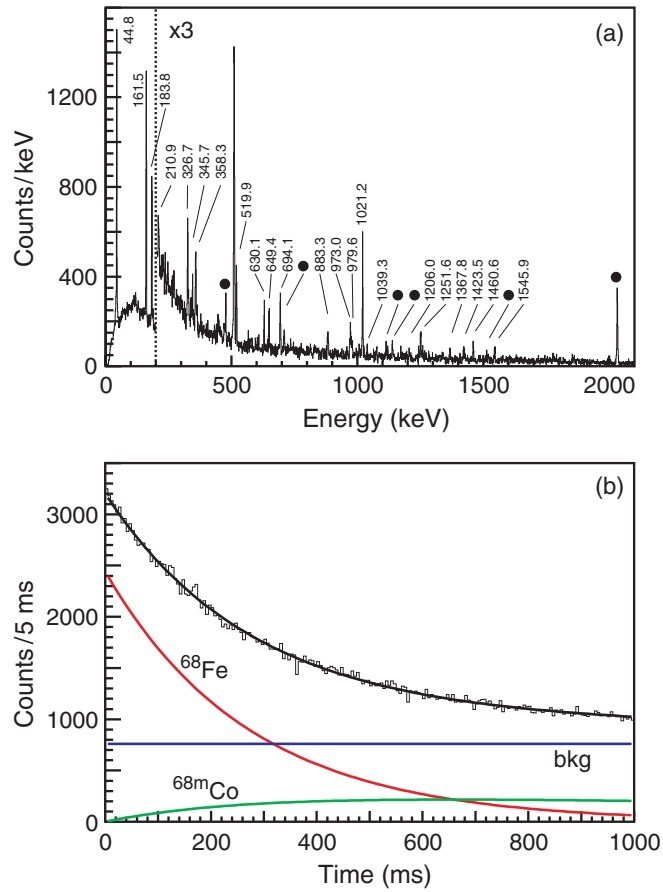

FIG. 5. (Color online) (a) The beta-delayed gamma-ray spectrum detected within 1 second of a ^{68}Fe implanted ion. Gamma rays following the decay of ^{68}Fe are marked with their respective energies. All other gamma rays were attributed to daughter transitions and are marked with circles. (b) The decay curve for ^{68}Co from 0 to 1 second. The overall fit to the decay curve (black) included contributions from the decay of ^{68}Fe (red), the low-spin ^{68}Co isomer (green), and a constant background (blue). See text for details.

in Table III, which led to the construction of the level scheme presented in Fig. 6.

The multipolarity of the 45-keV transition can be deduced from inferred electron conversion coefficients, derived from gamma-gamma coincidence spectra, and Weisskopf estimates. The gamma-ray spectrum in coincidence with the 184-keV transition is shown in Fig. 7. The 184-keV was chosen as a gating transition to isolate the 162-45 gamma-ray cascade (see Fig. 7). If the 45-keV state decayed exclusively through gamma-ray emission, the gamma-ray intensities at 45 keV and 162 keV in Fig. 7 would be equivalent, after correcting for the efficiency of SeGA (10% at 45 keV and 20% at 162 keV). The experimental ratio between 185-45 and 162-45 coincidences, after correcting for detection efficiencies, is 0.50(13) and is consistent amongst the gamma-ray transitions that feed the 162-45 cascade. This results in an inferred electron conversion coefficient of 1.0(4) which suggests either an $E1$ or $M1$ multipolarity assignment for the 45-keV transition. The expected conversion coefficient for either a $E1$ or $M1$ 45-keV transition in Co is 0.52 or 0.37, respectively. Tabulated

TABLE II. Gamma-ray transitions identified following the beta decay of ^{68}Fe along with their respective absolute gamma-ray intensities.

E (keV)	Absolute intensity (%)	E (keV)	Absolute intensity (%)
44.8(3)	24(2)[a]	979.6(3)	1.1(4)
161.5(3)	10(1)	1021.2(3)	6.7(6)
183.8(3)	6.9(5)	1039.3(4)	0.5(2)
210.9(4)	1.5(4)	1206.0(4)	0.4(3)
326.7(3)	1.8(3)	1251.6(3)	1.8(4)
345.7(3)	0.9(2)	1367.8(5)	1.2(5)
358.3(4)	4(2)	1423.5(5)	1.5(4)
519.9(3)	2.7(3)	1460.6(4)	1.4(3)
630.1(3)	1.9(4)	1545.9(4)	1.4(4)
649.4(3)	1.8(4)	2615.3(5)	1.1(4)
694.1(3)	2.5(4)		
883.3(4)	1.8(1)		
973.0(3)	11(2)		

[a]Absolute intensity of the transition considering conversion electrons and gamma-ray emission is 48(9)%.

comparisons between measured $E1$ transition rates and Weiskopf estimates [36] suggest a hindrance of the $E1$ transition between 10^2 and 10^6, albeit for heavier nuclei. Assuming a hindrance of 10^4 for the 45-keV transition would lead to a half-life estimate of ∼50 ns which was unfortunately below the experimental sensitivity.

Using the absolute gamma-ray intensities presented in Table II and the number of detected decay electrons the beta-decay branching ratios can be determined to each level and are presented on the left of Fig. 6 along with apparent log ft values. There is a large apparent, direct beta-decay transition between ^{68}Fe and the populated lower-spin isomeric state of ^{68}Co. As a result, the isomeric state in ^{68}Co is reassigned a tentative spin and parity of 1^+. The spin and parity of the 45-keV state is difficult to determine due to conflicting experimental data. An $E1$ multipolarity assignment based on the inferred electron conversion coefficient is suggestive of a 2^- spin and parity assignment mimicking the two lowest energy states observed in the $N = 41$ isotone, ^{66}Mn [20]. However, such an assignment is at odds with the large apparent beta-decay feeding to the 45-keV state. It should also be noted that the beta-decay feedings presented here are upper limits due to the lack of experimental sensitivity to low-intensity, high-energy gamma-ray transitions. Seven gamma rays listed in Table II were not placed in the level scheme, and account

TABLE III. Gamma-gamma coincidences observed following the beta decay of ^{68}Fe.

E (keV)	Coincident transitions (keV)
45	162, 184, 327, 346, 630, 649
161	45, 184, 358, 630, 1205
184	45, 162, 630
211	45, 161
326	45, 162, 184, 649, 694
346	45
358	45, 162
520	1027, 1251
630	45, 162, 184
649	45, 327
694	327
1251	520

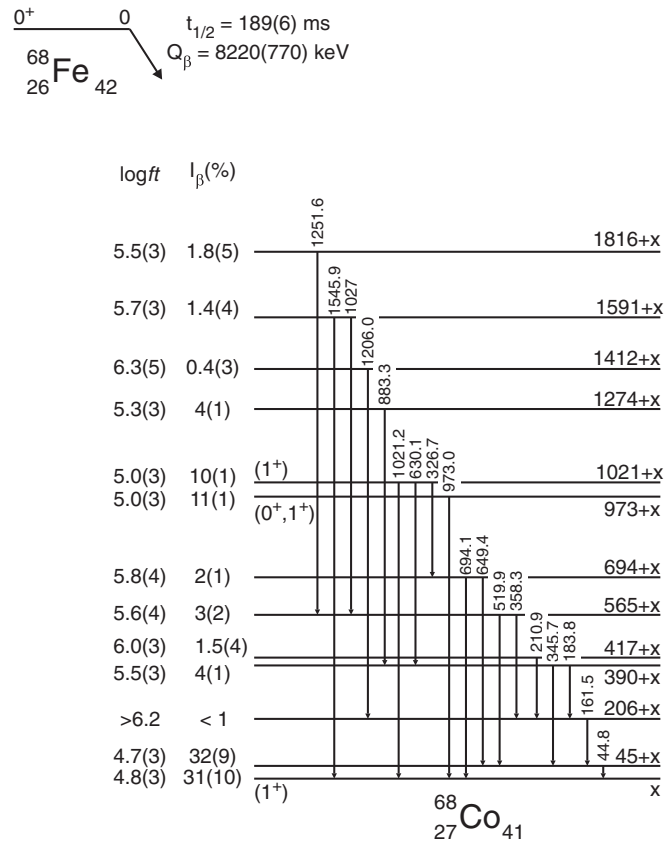

FIG. 6. Low-energy level structure of ^{68}Co populated in the decay of ^{68}Fe. The excitation energy of the isomer relative to the ground state is not known therefore all levels are offset by an unknown energy x. Tentative spin and parity assignments are proposed for a few levels. Beta-decay branching ratios and apparent log ft values are give to the left of each state. The ^{68}Co beta-decay Q value was taken from Ref. [34]. The log ft calculations assumed $x = 0$ keV.

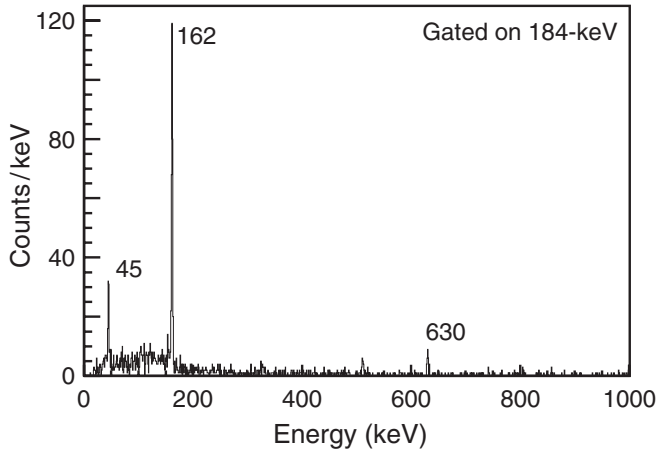

FIG. 7. Gamma-ray coincidence spectrum gated on the 184-keV transition following the beta decay of ^{68}Fe.

for a total absolute intensity of ∼8%. Due to the uncertainty, no spin and parity assignment is suggested for the 45-keV state.

Similar to ^{66}Co, there is a large beta-decay feeding to two excited states at $973 + x$ keV and $1021 + x$ keV in ^{68}Co suggestive of either a 1^+ or 0^+ spin and parity assignment. A tentative 1^+ assignment for the $1021 + x$-keV state is preferred and discussed further in Sec. IV.

IV. DISCUSSION

The coexistence of spherical and deformed shapes has been suggested for multiple nuclei near $N = 40$ starting with the odd-A ^{65,67}Co nuclei [19,22]. The coexistence phenomenon persists into the odd-odd ^{64,66}Mn isotopes wherein excited spherical isomeric states were observed a few hundred keV above the deformed ground states [20]. The specific neutron and proton orbitals responsible for the low-energy level structure in ^{66}Co and ^{68}Co can be inferred from the spherical and deformed configurations identified in neighboring odd-A nuclei in the Ni, Co, and Fe isotopic chains.

The spherical proton levels can be deduced from odd-A Co isotopes. The isolation of the proton $f_{7/2}$ single-particle state and the resultant $Z = 20$ and $Z = 28$ shell closures restrict spherical proton configurations below $_{28}$Ni to those involving holes in the $\pi f_{7/2}$ state. As evidence, the ground-state spin and parity of all odd-A Co isotopes are assigned as $7/2^-$.

The spherical neutron single-particle states and their relative energies can be extracted from the low-energy level schemes of ^{67}Ni and ^{69}Ni shown in Fig. 8. In a simple, extreme single-particle model, the low-energy levels can be attributed to neutron excitations amongst the three single-particle states; $p_{1/2}$, $f_{5/2}$, and $g_{9/2}$. In $^{67}_{28}$Ni$_{39}$, levels with J^π of $1/2^-$, $5/2^-$ and $9/2^+$ are observed at 0, 694, and 1007 keV respectively [37,38]. The spin and parity sequence of the lowest three excited levels of $^{69}_{28}$Ni$_{41}$ is $9/2^+$, $1/2^-$, and $5/2^-$ at excitation energies of 0, 321, and 915 keV, respectively. The low-energy levels observed in ^{67}Ni and ^{69}Ni set the relative ordering of the spherical neutron single-particle states in ascending energy; $f_{5/2}$, $p_{1/2}$, and $g_{9/2}$. Further, the energy necessary to to promote a neutron from the $f_{5/2}$ into the $p_{1/2}$ single-particle state is on the order of 600 keV based on the energy separation between the $1/2^-$ and $5/2^-$ states in both Ni nuclei. Thus, assuming a spherical nuclear shape, the 39th and 41st neutron in ^{66}Co and ^{68}Co would be expected in the neutron $p_{1/2}$ and $g_{9/2}$ single-particle state, respectively.

The salient deformed proton configurations are inferred from the low-energy states identified in odd-A Co isotopes and the Nilsson diagram shown in Fig. 8. A low-energy $1/2^-$ isomeric state was observed at 492 keV in ^{67}Co and was interpreted as a prolate-deformed shape isomer above the spherical $7/2^-$ ground state [19]. Indeed, at moderate prolate deformations around 0.2, a [321]1/2 level, originating from the spherical $p_{3/2}$ single-particle state, can be expected from the Nilsson diagram shown in Fig. 8. A similar [321]1/2 proton excitation has also been identified in ^{65}Co [22].

The accessible deformed neutron levels are identified from Fig. 8 based on a deformation of ∼0.2 used to interpret the low-energy level structure of ^{67}Fe [8]. The most important levels are the [301]1/2 and [431]3/2 originating from the $p_{1/2}$ and $g_{9/2}$ single-particle states, respectively. However, it should be noted that around $N = 40$ at the prolate deformations indicated in Fig. 8 there are numerous level crossings and different models provide slight variations on the relative energy separations between the available neutron orbitals [8,20,39].

A. ^{66}Co

The ground state of ^{66}Co was previously assigned a 3^+ spin and parity and attributed to the spherical $\pi f_{7/2}^{-1} \nu p_{1/2}^{-1}$ coupling [27], which would be expected from the removal of one proton from ^{67}Ni. However, a 3^+ spin and parity assignment for the ^{66}Co ground state is inconsistent with the observed beta-decay feeding pattern presented in Sec. II, and the ground state is reassigned as a 1^+ spin and parity. It is unlikely that the ^{66}Co ground state can be attributed to the spherical $\pi f_{7/2}^{-1} \nu f_{5/2}^{-1}$ coupling unless a switch in the ordering of the spherical neutron single-particle levels occurs with the removal of a proton from $^{67}_{28}$Ni$_{39}$ to $^{66}_{27}$Co$_{39}$. Instead, it is proposed that the ground state of ^{66}Co is deformed. The deformed ground state is the result of coupling the deformed proton [321]1/2 level observed in ^{67}Co with the [301]1/2 neutron state origination from the $\nu p_{1/2}$ resulting in a doublet of $1^+, 0^+$. The coupling rules of Ref. [40] predict the 1^+ would be the lowest in energy. A similar ground state configuration is observed in ^{64,66}Mn nuclei [20].

The 3^+ is tentatively assigned as the lowest energy spherical state in ^{66}Co and is interpreted as a member of the $\pi f_{7/2}^{-1} \nu p_{1/2}^{-1}$ doublet. The 4^+ state at 390 keV is an attractive candidate for the other member of the doublet. An alternative configuration leading to a 3^+ spin and parity would be the coupling of the deformed proton [321]1/2 with the neutron [303]5/2 resulting in a 2^+,3^+ doublet with the 3^+ state being lowest in energy [40]. However, from the beta-decay scheme shown in Fig. 4 the only likely candidate for the 2^+ member of the deformed doublet, at an energy of 510-keV, does not decay to the 3^+ as would be expected. Further, the long lifetime of the 175-keV $E2$ transition depopulating the 3^+ state can be explained as a transition between the spherical excited state and the deformed ground state.

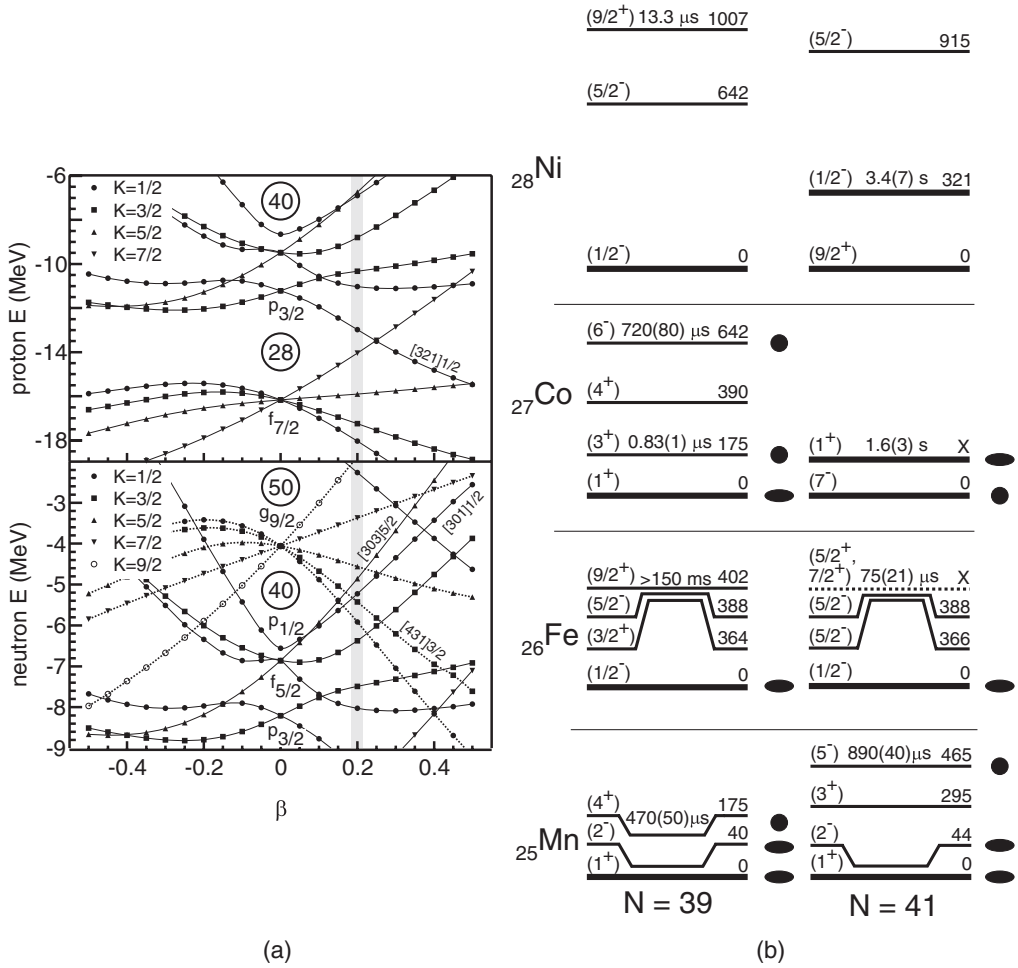

FIG. 8. (left) Proton and neutron single-particle levels calculated as a function of deformation. A vertical shaded region is placed at a deformation of $\beta = 0.2$. Selected states discussed in the text are labeled with asymptotic Nilsson quantum numbers. (right) Low-energy isomeric states and their decay paths for Co, Fe, and Mn nuclei along the $N = 39$ and $N = 41$ isotonic lines. Thick black lines indicate beta-decaying states. Deformed and spherical states for Mn, Fe, and Co nuclei are identified by either a circle or oval to the right of each state. Experimental data were taken from Refs. [14–16,20,27,33,41].

The state at 980 keV is tentatively associated with the spherical $\pi f_{7/2}^{-1}\nu f_{5/2}^{-1}$ configuration based on the lack of a direct transition to the deformed ground state and the observation of a direct transition to the previously identified 3^+ spherical state at 175 keV. The energy of the 980-keV state is ∼800 keV above the spherical $\pi f_{7/2}^{-1}\nu f_{5/2}^{-1}$ 3^+ state as expected based on the relative excitation of the $5/2^-$ and $1/2^-$ levels in the isotonic ^{67}Ni nucleus.

B. ^{68}Co

The ground state of ^{68}Co was previously assigned a spin and parity of 7^- and is attributed to the spherical $\pi f_{7/2}^{-1}$ and $\nu g_{9/2}^{+1}$ coupling [27]. The excited isomeric state previously identified as 3^+, has been reassigned a spin and parity of 1^+ based on the beta-decay data presented in Sec. III. Paralleling the argument for ^{66}Co, the 1^+ isomeric state in ^{68}Co is unlikely to be the spherical $\pi f_{7/2}^{-1}\nu f_{5/2}^{-1}$ configuration based on the relative excitation energies of the $5/2^-$ and $1/2^-$ levels in ^{69}Ni. Analogous to the ground states in both isotopic $^{66}_{27}Co_{39}$ and isotonic $^{66}_{25}Mn_{41}$ nuclei, it is proposed that the 1^+ state in ^{68}Co can be attributed to a deformed configuration involving the coupling of a [321]1/2 proton state with the [301]1/2 neutron level originating from the spherical $\pi p_{3/2}$ and $\nu p_{1/2}$, respectively.

Finally, there are two states at ∼1 MeV that are significantly fed in the beta decay of ^{68}Fe. Again, similar to ^{66}Co, the state at 1021 keV is suggested to be a 1^+ level originating from the spherical $\pi f_{7/2}\nu f_{5/2}$ single-particle coupling. The 1021-keV state lacks a direct transition to the deformed 1^+ state at $0 + x$ keV and is at a comparable energy to the $5/2^-$ excitation in ^{69}Ni, relative to the spherical ground state.

C. $N = 39$, $N = 41$ isotones

The isomeric states along the $N = 39$ and $N = 41$ isotones of Co, Fe, and Mn are presented in Fig. 8. In all four odd-Z isotopes shown in Fig. 8, ^{66,68}Co and ^{64,66}Mn, there is a

low-energy 1^+ state that is tentatively assigned as a deformed configuration involving the coupling of the proton [321]1/2 and the neutron [301]1/2 originating from the $\pi p_{3/2}$ and $\nu p_{1/2}$, respectively. The configuration is the ground state in ^{66}Co, ^{64}Mn, and ^{66}Mn and a low-energy isomeric state in ^{68}Co. The two neutron states, [301]1/2 and [431]3/2, originating from the $\nu p_{1/2}$ and $\nu g_{9/2}$ single-particle levels, respectively, are almost degenerate at the deformation of 0.2, assumed in the present analysis, and slight shifts to the neutron orbits are required to account for the fact that the [301]1/2 state appears to be the ground state neutron configuration at $N = 39$ and $N = 41$. The $1/2^-$ ground state spin and parity assignment to both $^{65}_{26}\mathrm{Fe}_{39}$ and $^{68}_{26}\mathrm{Fe}_{41}$ nuclei provide reasonable justification for the neutron [301]1/2 state remaining involved in the ground-state configuration in both the $N = 39$ and $N = 41$ isotones.

In each of the ^{66,68}Co and ^{64,66}Mn nuclei spherical states have also been identified. In the $N = 39$ isotones ^{66}Co and ^{64}Mn, a spherical isomeric states have been identified at an excitation energy of ∼175 keV above the ground state and attributed to the spherical coupling of the $\pi f_{7/2}$ and $\nu p_{1/2}$ single particle states. Along the $N = 41$ isotones comparable spherical states are identified as originating from the coupling of the $\pi f_{7/2}$ and $\nu g_{9/2}$. The spherical coupling of the $\pi f_{7/2}$ and $\nu f_{5/2}$ states resulting in a 1^+ spin and parity level are identified in all four nuclei at an energy around 1 MeV.

V. CONCLUSION

The low-energy level structures of ^{66}Co and ^{68}Co were populated through the beta decay of ^{66}Fe and ^{68}Fe respectively. In both ^{66}Co and ^{68}Co, the lowest energy populated state was reassigned from 3^+ to 1^+ spin and parity and attributed to a deformed configuration involving the coupling of a [321]1/2 proton with a [301]1/2 neutron originating from the $\pi p_{3/2}$ and $\nu p_{1/2}$ configurations. The states originating from the spherical coupling of the proton $f_{7/2}$ with either the neutron $p_{1/2}$ or $f_{5/2}$ single-particle states were identified. The coexistence of the two competing nuclear shapes is similar between the $N = 39$ and $N = 41$ isotones of Co and Mn nuclei.

ACKNOWLEDGMENTS

This work was funded in part by the NSF under Contracts No. PHY-0606007 and No. PHY-1102511 (NSCL) and the DOE under Contracts No. DE-FG02-96ER40983 (UT), No. DE-AC05-00OR22725 (ORNL), and No. DE-AC05-060R23100 (ORAU), and in part by the National Nuclear Security Administration under the Stewardship Science Academic Alliances program through DOE Cooperative Agreement No. DE-FG52-08NA28552.

[1] M. Bernas, P. Dessagne, M. Langevin, J. Payet, F. Pougheon, and P. Roussel, Phys. Lett. B **113**, 279 (1982).
[2] R. Broda, B. Fornal, W. Królas, T. Pawłat, D. Bazzacco, S. Lunardi, C. Rossi-Alvarez, R. Menegazzo, G. de Angelis, P. Bednarczyk, J. Rico, D. De Acuña, P. J. Daly, R. H. Mayer, M. Sferrazza, H. Grawe, K. H. Maier, and R. Schubart, Phys. Rev. Lett. **74**, 868 (1995).
[3] O. Sorlin, S. Leenhardt, C. Donzaud, J. Duprat, F. Azaiez, F. Nowacki, H. Grawe, Z. Dombrádi, F. Amorini, A. Astier, D. Baiborodin, M. Belleguic, C. Borcea, C. Bourgeois, D. M. Cullen, Z. Dlouhy, E. Dragulescu, M. Górska, S. Grévy, D. Guillemaud-Mueller, G. Hagemann, B. Herskind, J. Kiener, R. Lemmon, M. Lewitowicz, S. M. Lukyanov, P. Mayet, F. de Oliveira Santos, D. Pantalica, Y.-E. Penionzhkevich, F. Pougheon, A. Poves, N. Redon, M. G. Saint-Laurent, J. A. Scarpaci, G. Sletten, M. Stanoiu, O. Tarasov, and C. Theisen, Phys. Rev. Lett. **88**, 092501 (2002).
[4] A. Azaiez, Phys. Scr., T **88**, 118 (2000).
[5] P. Federman and S. Pittel, Phys. Lett. B **69**, 385 (1977).
[6] R. F. Casten, D. D. Warner, D. S. Brenner, and R. L. Gill, Phys. Rev. Lett. **47**, 1433 (1981).
[7] S. M. Lenzi, F. Nowacki, A. Poves, and K. Sieja, Phys. Rev. C **82**, 054301 (2010).
[8] J. M. Daugas, I. Matea, J.-P. Delaroche, M. Pfutzner, M. Sawicka, F. Becker, G. Belier, C. R. Bingham, R. Borcea, E. Bouchez, A. Buta, E. Dragulescu, G. Georgiev, J. Giovinazzo, M. Girod, H. Grawe, R. Grzywacz, F. Hammache, F. Ibrahim, M. Lewitowicz, J. Libert, P. Mayet, V. Meot, F. Negoita, F. de Oliveira Santos, O. Perru, O. Roig, K. Rykaczewski, M. G. Saint-Laurent, J. E. Sauvestre, O. Sorlin, M. Stanoiu, I. Stefan, Ch. Stodel, Ch. Theisen, D. Verney, and J. Zylicz, Phys. Rev. C **83**, 054312 (2011).
[9] O. Sorlin, C. Donzaud, L. Axelsson, M. Belleguic, R. Béraud, C. Borcea, G. Canchel, E. Chabanat, J. Daugas, A. Emsallem, D. Guillemaud-Mueller, K.-L. Kratz, S. Leenhardt, M. Lewitowicz, C. Longour, M. Lopez, F. de Oliveira Santos, L. Petizon, B. Pfeiffer, F. Pougheon, M. Saint-Laurent, and J. Sauvestre, Nucl. Phys. A **660**, 3 (1999).
[10] M. Girod, P. Dessagne, M. Bernas, M. Langevin, F. Pougheon, and P. Roussel, Phys. Rev. C **37**, 2600 (1988).
[11] M. Hannawald, T. Kautzsch, A. Wöhr, W. B. Walters, K.-L. Kratz, V. N. Fedoseyev, V. I. Mishin, W. Böhmer, B. Pfeiffer, V. Sebastian, Y. Jading, U. Köster, J. Lettry, H. L. Ravn, and the ISOLDE Collaboration, Phys. Rev. Lett. **82**, 1391 (1999).
[12] A. Gade, R. V. F. Janssens, T. Baugher, D. Bazin, B. A. Brown, M. P. Carpenter, C. J. Chiara, A. N. Deacon, S. J. Freeman, G. F. Grinyer, C. R. Hoffman, B. P. Kay, F. G. Kondev, T. Lauritsen, S. McDaniel, K. Meierbachtol, A. Ratkiewicz, S. R. Stroberg, K. A. Walsh, D. Weisshaar, R. Winkler, and S. Zhu, Phys. Rev. C **81**, 051304 (2010).
[13] S. J. Freeman, R. V. F. Janssens, B. A. Brown, M. P. Carpenter, S. M. Fischer, N. J. Hammond, M. Honma, T. Lauritsen, C. J. Lister, T. L. Khoo, G. Mukherjee, D. Seweryniak, J. F. Smith, B. J. Varley, M. Whitehead, and S. Zhu, Phys. Rev. C **69**, 064301 (2004).
[14] M. Block, C. Bachelet, G. Bollen, M. Facina, C. M. Folden, C. Guenaut, A. A. Kwiatkowski, D. J. Morrissey, G. K. Pang, A. Prinke, R. Ringle, J. Savory, P. Schury, and S. Schwarz, Phys. Rev. Lett. **100**, 132501 (2008).
[15] M. Sawicka, J. Daugas, H. Grawe, S. Cwiok, D. Balabanski, R. Béraud, C. Bingham, C. Borcea, M. La Commara, G. de France, G. Georgiev, M. Górska, R. Grzywacz, M. Hass, M. Hellström, Z. Janas, M. Lewitowicz, H. Mach, I. Matea,

G. Neyens, C. O' Leary, F. de Oliveira Santos, R. Page, M. Pfützner, Z. Podolyák, K. Rykaczewski, M. Stanoiu, and J. Zylicz, Eur. Phys. J. A **16**, 51 (2003).

[16] R. Grzywacz, R. Béraud, C. Borcea, A. Emsallem, M. Glogowski, H. Grawe, D. Guillemaud-Mueller, M. Hjorth-Jensen, M. Houry, M. Lewitowicz, A. C. Mueller, A. Nowak, A. Płochocki, M. Pfützner, K. Rykaczewski, M. G. Saint-Laurent, J. E. Sauvestre, M. Schaefer, O. Sorlin, J. Szerypo, W. Trinder, S. Viteritti, and J. Winfield, Phys. Rev. Lett. **81**, 766 (1998).

[17] C. J. Chiara, I. Stefanescu, N. Hoteling, W. B. Walters, R. V. F. Janssens, R. Broda, M. P. Carpenter, B. Fornal, A. A. Hecht, W. Królas, T. Lauritsen, T. Pawłat, D. Seweryniak, X. Wang, A. Wöhr, J. Wrzesiński, and S. Zhu, Phys. Rev. C **82**, 054313 (2010).

[18] O. B. Tarasov, D. J. Morrissey, A. M. Amthor, T. Baumann, D. Bazin, A. Gade, T. N. Ginter, M. Hausmann, N. Inabe, T. Kubo, A. Nettleton, J. Pereira, M. Portillo, B. M. Sherrill, A. Stolz, and M. Thoennessen, Phys. Rev. Lett. **102**, 142501 (2009).

[19] D. Pauwels, O. Ivanov, N. Bree, J. Büscher, T. E. Cocolios, J. Gentens, M. Huyse, A. Korgul, Y. Kudryavtsev, R. Raabe, M. Sawicka, I. Stefanescu, J. Van de Walle, P. Van den Bergh, P. Van Duppen, and W. B. Walters, Phys. Rev. C **78**, 041307 (2008).

[20] S. N. Liddick, S. Suchyta, B. Abromeit, A. Ayres, A. Bey, C. R. Bingham, M. Bolla, M. P. Carpenter, L. Cartegni, C. J. Chiara, H. L. Crawford, I. G. Darby, R. Grzywacz, G. Gürdal, S. Ilyushkin, N. Larson, M. Madurga, E. A. McCutchan, D. Miller, S. Padgett, S. V. Paulauskas, J. Pereira, M. M. Rajabali, K. Rykaczewski, S. Vinnikova, W. B. Walters, and S. Zhu, Phys. Rev. C **84**, 061305 (2011).

[21] K. Heyde and J. L. Wood, Rev. Mod. Phys. **83**, 1467 (2011).

[22] D. Pauwels, O. Ivanov, N. Bree, J. Büscher, T. E. Cocolios, M. Huyse, Y. Kudryavtsev, R. Raabe, M. Sawicka, J. V. de Walle, P. VanDuppen, A. Korgul, I. Stefanescu, A. A. Hecht, N. Hoteling, A. Wöhr, W. B. Walters, R. Broda, B. Fornal, W. Krolas, T. Pawlat, J. Wrzesinski, M. P. Carpenter, R. V. F. Janssens, T. Lauritsen, D. Seweryniak, S. Zhu, J. R. Stone, and X. Wang, Phys. Rev. C **79**, 044309 (2009).

[23] D. J. Morrissey, B. M. Sherrill, M. Steiner, A. Stolz, and I. Wiedenhoever, Nucl. Instrum. Methods Phys. Res. B **204**, 90 (2003).

[24] J. I. Prisciandaro, A. C. Morton, and P. F. Mantica, Nucl. Instrum. Methods Phys. Res. A **505**, 140 (2003).

[25] W. F. Mueller, J. A. Church, T. Glasmacher, D. Gutknecht, G. Hackman, P. G. Hansen, Z. Hu, K. L. Miller, and P. Quirin, Nucl. Instrum. Methods Phys. Res. A **466**, 492 (2001).

[26] K. Starosta, C. Vaman, D. Miller, P. Voss, D. Bazin, T. Glasmacher, H. Crawford, P. Mantica, H. Tan, W. Hennig, M. Walby, A. Fallu-Labruyere, J. Harris, D. Breus, P. Grudberg, and W. Warburton, Nucl. Instrum. Methods Phys. Res. A **610**, 700 (2009).

[27] W. F. Mueller, B. Bruyneel, S. Franchoo, M. Huyse, J. Kurpeta, K. Kruglov, Y. Kudryavtsev, N. V. S. V. Prasad, R. Raabe, I. Reusen, P. VanDuppen, J. V. Roosbroeck, L. Vermeeren, L. Weissman, Z. Janas, M. Karny, T. Kszczot, A. Pochocki, K.-L. Kratz, B. Pfeiffer, H. Grawe, U. Köster, P. Thirolf, and W. B. Walters, Phys. Rev. C **61**, 054308 (2000).

[28] S. Czajkowski, M. Bernas, P. Armbruster, H. Geissel, C. Kozhuharov, G. Munzenberg, D. Vieira, P. Dessagne, C. Miehe, E. Hanelt, G. Audi, and J. K. P. Lee, Z. Phys. A **348**, 267 (1994).

[29] S. Leenhardt, F. Azaiez, O. Sorlin, M. Belleguic, C. Bourgeois, C. Donzaud, J. Duprat, S. Grévy, D. Guillemaud-Mueller, A. Mueller, F. Pougheon, I. Deloncle, J. Kiener, M. Porquet, J. Daugas, M. Lewitowicz, F. de Oliveira, M. Saint-Laurent, J. Winfield, J. Angélique, N. Orr, A. Gillibert, F. Marie, C. Borcea, Y.-E. Penionzhkevich, Y. Sobolev, R. Béraud, G. Canchel, E. Chabanat, A. Emsalem, C. Longour, and J. Sauvestre, Nucl. Phys. A **654**, 683c (1999).

[30] F. Ameil, M. Bernas, P. Armbruster, S. Czajkowski, P. Dessagne, H. Geissel, E. Hanelt, C. Kozhuharov, C. Miehe, C. Donzaud, A. Grewe, A. Heinz, Z. Janas, M. de Jong, W. Schwab, and S. Steinhäuser, Eur. Phys. J. A **1**, 275 (1998).

[31] D. Pauwels, Proceedings of the First International Conference on Advances in Radioactive Isotope Science (unpublished).

[32] W. Darcey, R. Chapman, and S. Hinds, Nucl. Phys. A **170**, 253 (1971).

[33] G. Georgiev, Ph.D. thesis, Katholieke Universiteit Leuven, 2001 (unpublished).

[34] G. Audi, A. Wapstra, and C. Thibault, Nucl. Phys. A **729**, 337 (2003), the 2003 NUBASE and Atomic Mass Evaluations.

[35] O. Sorlin, C. Donzaud, F. Azaiez, C. Bourgeois, L. Gaudefroy, F. Ibrahim, D. Guillemaud-Mueller, F. Pougheon, M. Lewitowicz, F. de Oliveira Santos, M. Saint-Laurent, M. Stanoiu, S. Lukyanov, Y. Penionzhkevich, J. Angélique, S. Grévy, K.-L. Kratz, B. Pfeiffer, F. Nowacki, Z. Dlouhy, and J. Mrasek, Nucl. Phys. A **719**, C193 (2003).

[36] C. F. Perdristat, Rev. Mod. Phys. **1**, 41 (1966).

[37] T. Pawlat, R. Broda, W. Królas, A. Maj, M. Zięblíński, H. Grawe, R. Schubart, K. H. Maier, J. Heese, H. Kluge, and M. Schramm, Nucl. Phys. A **574**, 623 (1994).

[38] L. Weissman, A. Andreyev, B. Bruyneel, S. Franchoo, M. Huyse, K. Kruglov, Y. Kudryavtsev, W. F. Mueller, R. Raabe, I. Reusen, P. Van Duppen, J. Van Roosbroeck, L. Vermeeren, U. Köster, K. L. Kratz, B. Pfeiffer, P. Thirolf, and W. B. Walters, Phys. Rev. C **59**, 2004 (1999).

[39] P. Möller, J. R. Nix, and K. L. Kratz, At. Data Nucl. Data Tables **66**, 131 (1997).

[40] C. J. Gallagher and S. A. Moszkowski, Phys. Rev. **111**, 1282 (1958).

[41] J. I. Prisciandaro, P. F. Mantica, A. M. Oros-Peusquens, D. W. Anthony, M. Huhta, P. A. Lofy, and R. M. Ronningen, Phys. Rev. C **60**, 054307 (1999).